Removal of Rare Earth Metal Ions from Contaminated Water by Sustainable Carboxycellulose Nanofibers Derived from Agave through the Nitro Oxidation Process

Isha Brahmbhatt

Abstract

There is a growing need for rare earth metals such as lanthanides for use in electronic, medical, and nuclear applications. These precious metals, currently obtained through mining, contribute to contaminating nearby water sources. In this study, lanthanide ions were removed from solution by carboxycellulose nanofibers (CNF) derived from raw agave biomass. The nitro oxidation method was modified to convert raw agave biomass to agave CNF in a one-step process using nitric acid and sodium nitrite. This method was confirmed by characterizing agave CNF in terms of bonding, morphology, and composition. SEM measurements showed that the fibers contain visible fibrous structures. The TEM measurements of the fibers recorded average fiber lengths of 122.28-359.758 nm and average fiber widths of 5-6 nm, and AFM data displayed an average thickness of 1.6 nm. The oxidation of the agave CNF was confirmed with ^{13}C CPMAS NMR data. Zeta potential indicated that agave CNF had a highly negative surface (-117.3 mV), and the conductometric titration method revealed that the fibers had a high carboxylate content (0.75 mmol/g), confirming viability of agave CNF as a lanthanide removal agent. Evaluation of lanthanide ion removal by agave CNF from controlled samples caused a floc formation between the lanthanide ions and agave CNF. The Langmuir and Freundlich isotherms generated from ICP-MS studies indicated a 285.7 mg/g adsorption capacity and over a 90% adsorption efficiency for all tested lanthanide ion concentrations, which exceeds current water purification mechanisms such as iron oxide beads. Additionally, recovering the lanthanide ions from the flocculation had over a 60% efficiency for the tested lanthanide ion concentration, opening a new path of further studies and applications. These results suggest that nitro oxidized agave carboxycellulose nanofibers are a sustainable and effective alternative mechanism for water purification by removing and recovering the toxic but valuable lanthanide ions.

1. Introduction

The long-standing water contamination problem has left 785 million people globally without access to clean drinking water[6]. The increased production of lanthanides due to their good electrical, optical, and metallurgical properties is rapidly contributing to this problem[21]. Lanthanides are part of the rare earth elements, whose annual production is surpassing 120,000 tons a year for use in televisions, superconductors, plastic magnets, and ceramics[13,28]. As lanthanides compose less than 1% of Earth's crust, current methods of producing lanthanides are highly intensive and damaging to the environment. When released in nature, lanthanide ores can cause water pollution, loss of arable land, and increase mortality rates of aquatic and terrestrial organisms. In humans, lanthanides have an effect on metabolism and are highly toxic, similar to lead or cadmium. Pneumoconiosis and progressive restriction of the respiratory function have been associated with lanthanide exposure[28]. The majority of lanthanide production occurs in China, Japan, and India through mining ventures in rural areas[10]. Mining requires impurity removals through methods such as ion exchange, solvent extraction, and chlorination process, all of which are highly sensitive[24]. Villagers of Baotou, China evacuated in 2012 after years of being China's primary producer of lanthanides due to destruction of nearby vegetation, poor air quality, and the contamination of every nearby water source including a massive, murky lake that continues to release toxic fumes[16]. Furthermore, there are limited attempts to recycle, because the required treatments are costly and inaccessible[8]. This means that there are increased mining ventures to keep up with the rising demand for lanthanides in technologies, and consequently increased public exposure to the lanthanides, both from various commercial products and from production wastes/effluents[21].

Many current mechanisms of removing lanthanides from water sources involve expensive, advanced technologies that are difficult to implement in the primarily rural communities that mine for lanthanides. Review of water treatment technologies highlighted the cost barrier linked with new, large-scale filtration mechanisms[20]. On the other hand, small-scale methods used for water purification like chemical precipitation and electrocoagulation have higher efficiency at a lower cost, but often have artificial and environmentally damaging side effects like excessive toxic sludge production[25]. As the demand for lanthanides continues to grow, there will be increased demand to treat the consequent water contamination. Developing sustainable materials and procedures for the new, long-term water problems caused by the lanthanide production is an important gap in literature to address in response to rising environmental challenges today.

An alternate method of removing lanthanides is through carboxycellulose nanofibers (CNF), which are negatively charged chelation agents extracted from biomass, or plant waste[34]. A notable feature of CNF are the nanoscale structure of CNF, which is formed from the cellulose microfibrils in the cell

wall. Additionally, CNF has negative charges on the nanocellulose surface which is acquired by oxidizing the C6 position of the cellulose component in the plant biomass which acts as a functional group for further chemical reactions. As lanthanides are typically found in water as M^{3+} ions, the use of negatively charged materials can be an effective method to remove these ions from solution. The functional groups of CNF would bind to the lanthanide cations and remove them from solution in water purification mechanisms. As depicted in Figure 1, CNF is a derivative of cellulose, which is a renewable biopolymer that is often considered the most abundant polymer in nature[21,34]. CNF overcomes the limitations posed by expensive and environmentally harmful water purification mechanisms by utilizing a sustainable plant source and upcycling waste materials.

CNF can be extracted from a variety of plant biomass. I decided to work with agave biomass because agave is invasive species with large growth in areas that are the main producers of lanthanides. Wood, jute fibers, dried hemp, and cotton biomass were also considered. However, cotton biomass is typically recycled and prevalently utilized in the lanthanide producing regions of India and China[18], and wood, jute fibers, and dried hemp biomass have lower cellulose content than agave biomass[9,26]. This makes agave an accessible and efficient material for communities that require lanthanide removal mechanisms[19]. Approximately 66% of agave biomass is discarded or burned due to its limited value[3,5], so extracting agave CNF would upcycle this underutilized waste material. Agave CNF represents a more sustainable and cost-effective solution for lanthanide contamination in water.

In addition to a sustainable source of CNF, there is a need for a sustainable method to extract CNF from raw agave biomass. Current methods of generating CNF include reducing biomass mixtures of cellulose, hemicellulose, lignin, and other impurities to cellulose with acids like HCl, followed by oxidation mechanisms like TEMPO-mediated oxidation, carboxymethylation, phosphorylation, acetylation, or silylation[12]. However, these mechanisms are often costly and require high chemical and water consumption. The one-step nitro oxidation process was developed in my mentor's lab and has been used to extract CNF from various plant biomass sources[32]. The nitro oxidation process improves upon the gaps in current methods, as while both TEMPO-mediated oxidation and nitro oxidation utilize biomass sources, nitro oxidation offers a lower cost alternative[37]. In this process, nitric acid and sodium nitrite simultaneously form salts with the lignin and hemicellulose in raw biomass, and oxidize the CH_2OH functional group into a COOH functional group at the C6 position on the cellulose to form nitro oxidized CNF. Furthermore, this process employs only two low-cost chemicals, nitric acid and sodium nitrite, in a one-step process that reduces chemical and water consumption as compared to the existing multi-step methods. After reading about this nitro oxidation process research conducted in my lab, I was drawn to exploring this sustainable process to extract CNF from agave biomass.

Although there are other heavy metal cations such as Pb^{3+} and Cd^{2+} that contaminate water, I chose to target water contamination by lanthanide ions in this study. While the nitro oxidation process produces CNF that can theoretically target any cation in solution, the use of lanthanide in medical, nuclear, and electric applications will continue to grow, making water contamination due to lanthanide ions a critical and growing problem[13,21]. Furthermore, lanthanide mining procedures are unrefined and crudely performed in rural communities that do not have the capacity to combat the consequent toxic and carcinogenic effects with advanced medical treatments. Thus, I viewed developing a lanthanide removal mechanism using accessible and sustainable materials as a pertinent area of study. Among lanthanides, I focused on lanthanum ions, La^{3+}, in this study. My lab is continuing to study three other lanthanide species, Eu^{3+}, Ne^{3+}, and Dy^{3+}, that require radioactivity and toxicity material permits that were challenging for me to obtain in my limited time working at the lab. The corresponding results will be included in the work we are publishing and will not be presented in this study.

2. Goals and Hypothesis

The goal of this study was to evaluate agave CNF as sustainable and viable La^{3+} ion removal agents in contaminated water. It was hypothesized that agave CNF would possess a high adsorption efficiency for La^{3+} ions while also being an accessible and sustainable material.

There were three main objectives:

2.1 The first objective was to synthesize CNF that possesses high carboxyl content and a negative surface from raw agave biomass using the one-step nitro oxidation process as a viable material to remove La^{3+} ions from contaminated water.

2.2 The second objective was to characterize the agave CNF in terms of its fiber morphology and chemical bonding properties.

2.3 The third objective was to evaluate the efficiency of agave CNF at removing La^{3+} ions from solution.

2.4 Finally, additional analysis was performed to evaluate the potential of recovering La^{3+} ions from the floc formed by the ions and the agave CNF.

3. Methodology

Agave biomass sources samples imported from India, Africa, and the Philippines were grounded to powder but left without any further treatment. Analytical grade nitric acid (ACS reagent, 65%) and sodium nitrite (ACS reagent ≥ 97 %) were purchased from Sigma Aldrich and sodium bicarbonate was purchased from Fisher Scientific. All chemicals were used without further purification.

3.1 Synthesis of Agave Carboxycellulose Nanofibers using the Nitro Oxidation Process

The nitro oxidation process outlined in my lab's published work on jute fibers biomass was adapted for agave biomass by comparing the nanofibers sizes of both materials[32]. After calculating a new set of procedure parameters with my mentor, I followed a similar protocol as the original nitro oxidation process. In this new procedure, 10 grams of raw agave biomass were placed in a three-neck round-bottom flask, and 12 mL of nitric acid was added to the sample. Under continuous stirring at 140 rpm, 4.8 grams of sodium nitrite were added to the reaction mixture, forming red fumes inside of the flask. In order to trap the fumes inside the flask and prevent them from escaping, the mouths of the flask were sealed with stoppers. The reaction lasted 12 hours performed at 60ºC, and its completion was marked by adding 250 mL of distilled water to the flask. The supernatant liquid in the flask was decanted to remove the excess step once the final product equilibrated, and this step was repeated 2-3 times until the fibers started to suspend in water. The recovered product was washed with water and centrifuged at 5000 X g for 10 minutes until the suspension's pH value was above 2.5. Then, the suspension was transferred to a dialysis bag, with water repeatedly being changed, for 4-5 days until the conductivity of the suspension reached below 5 S/m. After that, a bicarbonate treatment was performed to increase the dispersion of the nanofibers in water by treating the suspension 4 wt% sodium bicarbonate until the pH reached 8 and stabilized for 10 minutes. This step was performed to generate ionic charges in the carboxylate groups, and improve the CNF dispersion by converting the COOH functional groups to COONa groups. The subsequent procedures involving secondary dialysis and homogenization of the agave CNF are protected under lab's patent-pending application.

To measure the carboxyl content of CNF which in turn would help determine the CNF's ability to chelate La^{3+} ions from contaminated water, conductometric titration was performed. A suspension was formed by dispersing 0.3 grams of the dried samples in 55 mL of distilled water. While stirring for 15 minutes, 5 mL of NaCl was added to the suspension. The addition of 0.1 M HCl was added to the suspension to achieve a pH within a 2.5-3 range. Following that, 0.04M NaOH was added at a rate of 0.1 mL/min until the pH of the suspension reached to 11. The conductivity and pH curves were translated into the calculation of the carboxylate content.

To measure the degree of negativity of the CNF surface, which in turn would help determine the CNF's ability to chelate La^{3+} ions from contaminated water, I chose to perform zeta potential analysis. A Brookhaven NanoBrook Omni machine was used with BIC Particle Solutions software to measure the charge of agave CNF. The software took the average of 20 cycles of the measured velocity from pushing microfibrillated agave CNF through the machine and converted it to a measured voltage.

3.2 Characterization of Agave Carboxycellulose Nanofibers

To evaluate the change in bond lengths between the raw agave biomass and agave CNF, Fourier Transform Infrared Spectroscopy (FTIR) was performed. I looked for changes in OH and C-H stretching to confirm that the cellulose in the raw agave biomass was oxidized to form carboxycellulose. A Nicolet iS10 instrument was used to record FTIR curves in the diamond attenuated total reflectance (ATR) mode and take 60 scans between 450 and 4000 cm^{-1} at a resolution of 4 cm^{-1}.

Scanning electron microscopy (SEM) and Energy Dispersive X-Ray Spectroscopy (EDX) were performed on the CNF to further observe the changes in chemical composition between the raw agave biomass and agave CNF. While the raw agave biomass should contain a variety of impurities and chemical compounds, the agave CNF should have isolated the cellulose in the biomass.

The morphology of the agave CNF was observed using transmission electron microscopy (TEM) to measure fiber length and width, and atomic force microscopy (AFM) to measure fiber depth. To obtain TEM measurements, a FEI Tecnai G2 Spirit BioTWIN instrument was operated at an accelerating voltage of 120 kV and equipped with a digital camera to study agave CNF. The samples were prepared by depositing a 10 L aliquot sample of 1mg of 6-carboxycellulose in 10 mL distilled water on a freshly glow discharged carbon coated Cu grids. The agave CNF samples were stained with 2 wt% aqueous uranyl acetate to distinguish the fiber morphology. ImageJ software analysis techniques that I learned in my previous materials science research projects were used to measure the lengths and widths of individual fibers and calculate the average fiber length and width of agave CNF. A Bruker Dimension ICON scanning probe microscope equipped with a Bruker OTESPA tip with a maximum radius of 10 nm was used to obtain AFM measurements of raw agave biomass and agave CNF. The air-dried sample was measured in tapping mode once a 10L sample of the 0.005 wt % suspension was deposited on the surface of a silica plate. The machine yielded average fiber thickness values for the agave CNF.

To confirm the isolation of cellulose in the agave CNF from the raw agave biomass and the conversion of agave fibers to agave nanofibers, I chose to perform carbon-13 cross-polarization magic-angle spinning nuclear magnetic resonance spectroscopy (^{13}C CPMAS NMR). A Bruker Ultrashield 500WB plus (500MHz) NMR instrument was used to perform solid state ^{13}C CPMAS NMR on biomass fibers and CNF. The instrument was capable of spinning samples up to 35 Hz, and was equipped with 2.5 mm triple resonance magic angle spinning NMR probe. The agave CNF samples were spun at the magic angle with a speed of 10 kHz and measured at a resonance frequency of 10,000 Hz. Baselines were added to the spectra produced by the machine using Gaussian and Lorentzian standards in literature[1]. Raw agave biomass and agave CNF spectra were compared to identify peaks that confirmed

the conversion of raw agave biomass to agave CNF and reveal any trace residuals of lignin, hemicellulose, or other common impurities.

3.3 Evaluation of Lanthanide Ion Removal by Agave Carboxycellulose Nanofibers

The La^{3+} remediation studies were performed by the following procedures. The stock solutions of La^{3+} ions were mixed with water to form solutions with concentrations of La^{3+} ions from 10 ppm - 10,000 ppm. 3 mL of each La^{3+} ion concentration solution were combined with 3 mL of CNF suspension of 0.32 wt %. Bubbles formed upon mixing, attributed to a gelation effect, and a metallic 'floc' formed settled to the bottom due to mixing (Figure 6). The supernatant portion was diluted down to 100 ppb to prepare samples for further testing. The flocculated portion was separated using a 0.1 microL syringe filter.

The extracted portion of the flocculation was characterized using FTIR and SEM/EDX. FTIR was performed to measure any interactions between the La^{3+} ions and the COO^- ions in the agave CNF. The SEM/EDX was performed to confirm the lanthanum elemental peak in the flocculation and to observe changes on the fibrous structures of the agave CNF.

I also chose to perform rheological analysis on the floc to note its cross-linking properties after noticing gelation in the flocculation. My past research experience in materials science enabled me to consider other physical properties involved in the interaction between the agave CNF and La^{3+} ions. Although these properties do not directly contribute to the goal of our study, I took the opportunity to make these characterizations as they are important to explore prior to future implementation.

To evaluate the adsorption efficiency and capacity of the agave CNF, the extracted and diluted supernatant, which was diluted with 2 wt % nitric acid to 100 ppb, was characterized using the standard inductively coupled plasma mass spectrometry (ICP-MS) technique while maintaining the pH of the sample[21]. The difference between the adsorption of the La^{3+} ions before and after mixing with the CNF suspension was calculated to determine the adsorption efficiency. The adsorption capacity was determined by calculating both ideal capacity, based on the available La^{3+} ions and the available mass in grams of CNF in suspension, and the experimental adsorption capacity, the product of the adsorption efficiency and ideal adsorption capacity. The La^{3+} ion concentration also defined the function for the experimental adsorption capacity of the CNF.

The adsorption capacity and efficiency of the agave CNF was calculated by fitting the ICP-MS data to isotherms[15,2]. From previous literature involving negatively charged materials to remove cations, I chose to first fit the data to a Langmuir isotherm, which assumes an equivalent adsorption center. The Langmuir isotherm model, based on a monolayer adsorption on the active site of the adsorbent, was used to determine the maximum adsorption (removal capacity) of the CNF for La^{3+} ions. The linearized form of the Langmuir isotherm model is represented in Equation 1:

(1) $$\frac{C_e}{Q_e} = \frac{1}{K_L Q_m} + \frac{C_e}{Q_m}$$

where C_e (mg/L) is the equilibrium concentration of La^{3+} ions in solution, Q_e (mg/g) is the initial equilibrium concentration in adsorbent that corresponds to initial concentration in solution C_0 (mg/L), Q_m or Q_{max} (mg/g) is the maximum monolayer adsorption capacity and the adsorption capacity of La^{3+} ions by CNF at equilibrium, and K_L (L/mg) is the Langmuir constant. Equation 1 is represented by plotting $\frac{C_e}{Q_e}$ vs C_e. The plot is used to calculate slope, $\frac{1}{Q_m}$, and intercept, $\frac{1}{K_L Q_m}$, and the coefficient R^2 for the Langmuir isotherm model.

After comparing the high Q_m value with the low R^2 coefficient along with noting the high cross-linking properties of the floc from the rheological studies, I decided to also fit the data to a Freundlich isotherm. The Freundlich isotherm model is based on a multilayer adsorption model and assumes an infinite number of adsorption centers. The linearized form of the Freundlich isotherm model represented by Equation 2:

(2) $$\log Q_e = \log K_F + \frac{1}{n} \log C_e$$

where C_e (mg/L) is the equilibrium concentration of La^{3+} ions in solution, Q_e (mg/g) is the initial equilibrium concentration in adsorbent that corresponds to initial concentration in solution C_0 [mg/L]. In Equation 2, n is the Freundlich constant and K_f [$(mg^{1-\frac{1}{n}})(L^{\frac{1}{g}})$] is the Freundlich equilibrium coefficient that may be interpreted as relative indicators of adsorption energy and adsorption capacity, respectively[2]. Equation 2 is represented by plotting log Q_e vs log C_e. The plot is used to calculate the coefficient R^2 for the Freundlich isotherm model.

3.4 Recovery of Lanthanide Ions from Floc

An additional aspect I considered was the potential recovery of the La^{3+} ions from the flocculation formed by the agave CNF and La^{3+} ions as an added benefit of this method. As the La^{3+} ions were essentially stored within the flocculation, I selected dilute hydrofluoric acid treatment on the floc based on previous literature. This process would dissolve the agave CNF from the flocculation, and leave behind the La^{3+} ions that do not dissolve in hydrofluoric acid. Due to limited time and resources, I performed 6 trials of this recovery study on solutions of 500 ppm La^{3+} ions and agave CNF. The exact measurements of the hydrofluoric acid treatment on the floc are protected under lab confidentiality agreements. After the acid treatment, the remaining contents of the solution were diluted down to 100ppb and tested with ICP-MS studies. The recovery efficiency was calculated by dividing the La^{3+} detected in the floc solution through ICP-MS by the maximum La^{3+} ions contained in the floc. The percentage of adsorption efficiency was averaged for the 6 trials.

4. Results and Discussion

4.1 Confirmation of Synthesis of Agave Carboxycellulose Nanofibers

The conductometric titration method determined the synthesized agave CNF had a high carboxyl content of 0.75 mmol/g. Zeta potential analysis indicated the agave CNF had a highly negative surface of -117.3 mV. While CNF is known to have a negative charge, knowing the degree of negativity on the surface of the agave CNF produced in this study may be important in adapting the method established in this study for other toxic cation removal. The high carboxylate content and negative surface of the CNF confirm its potential application in removing La^{3+} ions from solution. This is because there are an increased number of carboxylate groups available to bind to the La^{3+} ions in solution and the highly negative charge of the agave CNF increases the attraction between the agave CNF and La^{3+} ions.

4.2 Characterization of Agave Carboxycellulose Nanofibers

The FTIR spectrum of raw agave biomass (Figure 2) has several distinctive peaks: 3331 cm^{-1}(OH stretching) and 2899 cm^{-1}(C-H symmetrical stretching) in the cellulose unit; 1600 cm^{-1}(C=C aromatic symmetrical stretching) in the lignin unit; 1730 cm^{-1}, 1490 cm^{-1}, 1290 $cm^{-1}$and 860 cm^{-1} in the xylan and glucomannan of hemicellulose units. There peaks caused by lignin and hemicellulose units were all greatly reduced or completely absent in the spectrum for agave CNF. The COONa peak at 1600 cm^{-1} increased while the peak from the C-H stretching at 2899 cm^{-1} in agave CNF decreased, confirming the oxidation of the anhydroglucose units at the C6 position. This is indicative of an effective removal of hemicellulose and lignin impurities in the raw agave biomass by the treatment of nitric acid and sodium nitrite, supporting the use of the nitro oxidation process for extracting agave CNF.

The SEM images of the raw agave biomass indicate the presence of cellulose as well as many impurities including hemicellulose and lignin (Figure 3A). This is supported by the EDX diagram which registers many elements aside from the organic components of biomass which are cellulose, lignin, hemicellulose (Figure 3B). In the SEM image of the agave CNF, there is a formation of visible fibers (Figure 3C). The composition of these fibers is revealed in the EDX diagram (Figure 3D). The C and O peaks confirm the isolation of cellulose, and the Na peak confirms the formation of COONa groups through the bicarbonate treatment in the nitro oxidation process. SEM/EDX confirms the effectiveness of the nitro oxidation process in converting raw agave biomass to agave CNF and supports the results obtained by the conductometric titration method and zeta potential analysis.

Typical TEM images of agave CNFare illustrated in Figure 4A. These images were used to estimate morphological data such as the average fiber length and width. It was found that most nanofibers possessed similar widths between 5 and 6 nm, and average lengths from 122.28 to 359.758 nm. AFM images of agave CNF are shown in Figure 4B, confirming fiber morphology and indicating that the

average thickness of agave nanofibers was around 1.6 nm. The morphology characterizations of agave CNF are consistent with the ranges of width, length, and thickness observed in previous studies on various types of CNF[7,14,29,11].

Solid state ^{13}C CPMAS NMR spectrum of agave CNF is shown in Figure 5. Notably, the C6 carbon of the primary alcohol group was identified in the cluster between 60 and 70 ppm. The C2, C3, and C5 carbons were assigned to the next region between 70 and 80 ppm. The C4 carbon was associated with the region between 80 and 95 ppm. The region between 100 and 110 ppm was attributed to the anomeric carbon C1. The assignment of these peaks was based on previous characterization of carboxycellulose nanomaterials[17]. There is a low intensity peak at 171-172 ppm that corresponds with lignin's C1 carbon guaiacyl units and C3 and C4 syringyl units, and there is a disappearance of distinct peaks belonging to hemicellulose. These results confirm the removal of the majority of lignin, hemicellulose, and other impurities present in raw agave biomass through the nitro oxidation process[1]. The ^{13}C CPMAS NMR analysis gives insight on the composition of agave CNF and also confirms the oxidation of the C6 position of cellulose and removal of impurities in raw agave biomass through the nitro oxidation process.

4.3 Evaluation of Lanthanide Ions Removal by Agave Carboxycellulose Nanofibers

To assess the adsorption efficiency of agave CNF, ICP-MS studies were performed on supernatant portion of solutions containing La^{3+} ions of various concentrations and agave CNF. The data was fitted to both the Langmuir and Freundlich isotherms in order to analyze adsorption patterns. There was a moderate R^2 coefficient with the Langmuir isotherm, which is associated with monolayer adsorption, that indicated a Q_{max} value of 285.7 mg/g (Figure 9A).

There was a high R^2 coefficient with the Freundlich isotherm, which is associated with multilayer adsorption (Figure 9B). Though the Freundlich isotherm does not yield a maximum adsorption capacity value, it gives K_f and n values that can be compared quantitatively without a measure of units. The higher effectiveness of agave CNF in La^{3+} removal than other materials in both adsorption isotherm models supports the use of agave CNF as a more effective La^{3+} removal material while also being a sustainable and highly accessible material. The agave CNF had over a 90% efficiency in La^{3+} ion adsorption for all concentrations of La^{3+} ion solutions tested (Figure 10).

The multilayer adsorption pattern of agave CNF was especially fascinating because it differs from the monolayer pattern of many existing cation removal agents. Rheological studies, discussed below, account for the cross-linking between La^{3+} ions and agave CNF that may have created a mesh through which multilayer adsorption occurred.

The adsorption capacity and efficiency of agave CNF was compared to existing methods for removing La^{3+} ions from solutions in literature. As displayed in Table 1, the synthesized agave CNF has a much higher adsorption capacity than any existing mechanism discussed in previous literature. Additionally, as displayed in Table 2, agave CNF has K_f and n values that are lower than those of existing materials. The comparison of K_f and n values in Table 2 requires further analysis through a kinetics model to be fully interpreted[2]. Overall, agave CNF is a more accessible and sustainable material that can be used to successfully remove La^{3+} ions than existing materials. This supports the environmental and toxicological benefits of using agave CNF as a sustainable material for La^{3+} removal in densely contaminated areas.

4.4 Characterization of Agave Carboxycellulose Nanofibers and Lanthanide Ions Floc

FTIR performed on the floc formed by La^{3+} ions revealed the chemical interaction between La^{3+} ions and agave carboxycellulose nanofibers (Figure 7). The peak at 1619 cm^{-1}, representing COO^-, broadened in the floc as compared to the agave CNF, indicating cross-linking between the agave CNF and La^{3+} ions. Similarly, the peak at 3332 cm^{-1}, associated with hydroxyl (-OH) stretching, was broader in the floc than the agave, suggesting the formation of lanthanum hydroxide which supports cross-linking. This confirms the interaction of La^{3+} ions with the functional groups on the surface of the agave CNF.

The SEM data for the floc shows the agglomeration of agave CNF which may be attributed to interaction with La^{3+} ions (Figure 8A). There are thick structures in the images of the floc taken at 500 ppm that are further indicative of lanthanum oxide formation. The presence of lanthanum on the surface is confirmed by EDX measurements (Figure 8B).

The low R^2 coefficient for the Langmuir isotherm and high R^2 coefficient for the Freundlich isotherm suggests that the agave CNF follows an adsorption pattern that extends through multiple layers. One possible explanation of this phenomenon in the suspension form of agave CNF is that a large amount of crosslinking occurred between the La^{3+} ions and the agave CNF while they were in solution. This hypothesis is supported by the visually observed gelation effect in the phials with high La^{3+} ion concentration. To confirm this, I performed rheological analysis of the agave CNF and La3+ ions solutions. The rheological analysis indicated that because of the negative charged surface, CNF could effectively attract the positive La^{3+} ions. However, the ionic strength could in turn affect the rheological properties of agave CNF. The static rheology result of agave CNF after absorbing La^{3+} ions is shown in Figure 11 for La^{3+} ions of concentrations of 2-50 ppm. Higher concentrations of La^{3+} were unable to be tested because the gel-like structures and inhomogeneity become viscous enough to trap the bubbles. First, all the agave CNF and La^{3+} ions flocs displayed shear thinning behavior, indicating that the samples behave similarly to the convention polymer solutions. Second, compared to agave CNF, the flocs had

increased viscosity because the added La^{3+} ions may have sheltered the surface charges of CNF[37]. In the lower concentrations of La^{3+} ions, the viscosity increment was less obvious. That may be because there are not enough La^{3+} ions to screen the agave CNF and cross-link the different agave CNF. When the concentration of La^{3+} reached 50 ppm, the viscosity increased dramatically. Moreover, because lanthanum has a valence charge of M^{3+}, La^{3+} may have been able to attract more than one COO^- group by acting as a cross-linking agent aside from only screening the charges. The effect of the agave CNF's concentration on its viscosity or overlap concentration may be mirrored by La^{3+} ions[37]; this hypothesis is under investigation.

4.5 Recovery of Lanthanide Ions from Floc

There was over a 60% efficiency in recovering La^{3+} ions from flocs of 500ppm La^{3+} ions and agave CNF for all 6 trials as evidenced by the ICP-MS studies. This is a substantial yield relative to the concentration of La^{3+} ions tested, so the recovery component of this study should be considered in terms of application. Rural communities who are currently mining for lanthanides may be able to use my approach to remove La^{3+} ion contaminants from their water sources. Although the recovery mechanism is not a replacement for mining, the ability to recover La^{3+} ions poses as another advantage of implementing this system. I am currently exploring this methodology through pseudo-first-order or second-order kinetics models and hope to incorporate it into prototypes my lab creates prior to implementation.

4.6 Future Research

A limitation of this study is that agave CNF were tested against solutions of varying concentrations of pure La^{3+} ions. In application, the agave CNF would be in a solution of an abundance of both cations and anions. Therefore, it is necessary to to test agave CNF in water samples from the same water sources that lanthanide mining communities typically access. As the mechanism of agave CNF in removing La^{3+} ions is based on electron bonding, agave CNF may be a viable removal agent for any cationic toxin. This is consistent with the removal of cadmium ions using CNF extracted from jute fibers in my lab's previous work, and needs to be confirmed with agave CNF[31].

Another important factor to consider prior to implementation would be confirming the mechanism of nitric acid and sodium nitrate in converting the raw biomass to CNF. My lab's previous work[32] supports a proposed mechanism of nitro oxidation depicted in Figure 12. Although nitric acid alone was effective at simultaneously fibrillating and oxidizing the agave, the yield to produce carboxycellulose nanofibers was relatively low even after 24 hrs of reaction. The addition of sodium nitrite appeared to play a synergistic role in enhancing the fibrillating and oxidizing ability of nitric acid. The reaction of sodium nitrite and nitric acid produces HNO_2, which serves as the true oxidation agent. The excess acid liberates nitrosonium ions (NO^+) from HNO_2 that target the primary hydroxyl group of

cellulose at the C6 position. The nitrosonium ions use an intermediate ester ($R\text{-}CH_2\text{-}O\text{-}NO$) that decomposes in an acidic medium to produce an aldehyde group and HNO on the C6 position of cellulose. The HNO is oxidized to HNO_2 under the excess acid, which causes the oxidation cycle to continue. As the reaction proceeds, the nitric acid is consumed and HNO self-dissociates into N_2O and water molecules. The aldehyde group completely oxidizes into the carboxyl group under the conditions of high reaction temperature (70º C) and high acid concentration. Additionally, the presence of nitric acid may have eliminated non-cellulose portions and non-crystalline cellulose components to initiate the fibrillation process of the raw agave biomass. This interaction between nitric acid and remaining crystalline cellulose regions leads to CNF of lower crystallinity. The crystallinity of the agave CNF created in this study can also be confirmed with Wide Angle X-Ray Diffraction (WAXD), which my mentor is planning to perform. However, the exact mechanism of nitric acid and sodium nitrite in oxidizing the C6 position of the cellulose in the raw agave biomass needs to be further explored to be confirmed.

I am currently attempting to perform a backreaction of the nitro oxidation process on the flocculation to recycle the agave CNF. This would further increases the sustainability advantage of agave CNF for La^{3+} ions removal, as it can be repeatedly reused in the method described in this study.

5. Conclusions

Carboxycellulose nanofibers (CNF) were successfully synthesized from raw agave biomass using the one-step nitro oxidation process. Various spectroscopy and analytical characterization techniques like FTIR, SEM/EDX, TEM, AFM, and ^{13}C CPMAS NMR confirmed the ability of the nitro oxidation process to form agave CNF, which possessed visible fibrous structures. The agave CNF had a highly negative surface (zeta potential -117.3 mV), and high carboxylate content (0.75 mmol/g). Agave CNF was a more effective material for La^{3+} removal as compared to existing removal mechanisms in literature, with over a 90% adsorption efficiency for all La^{3+} ion concentrations tested. It was interesting to note that La^{3+} ion removal by agave CNF had a stronger R^2 coefficient for the Freundlich isotherm, which represents multilayer adsorption. This adsorption pattern was further explored with rheological analysis that suggested cross-linking between the La^{3+} ions and agave CNF. There was over a 60% efficiency for the recovery of La^{3+} ions from the floc formed by agave CNF and La^{3+} ions. Future work will test the method demonstrated in this paper on site-based water samples and expand the cation recovery pathway to combat new water contamination challenges.

6. Figures and Tables

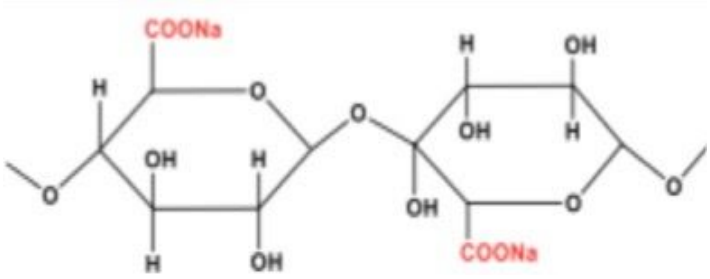

Figure 1. **Chemical Structure of Carboxycellulose Nanofibers (CNF).** Cellulose is the elementary unit component in plants, plant cells, secondary walls, fibers, macrofibrils, and microfibrils. CNF is formed by oxidizing the CH_2OH functional group to a COOH functional group at the C6 position of a cellulose molecule. The nitro oxidation process contains a bicarbonate treatment following the oxidation of the cellulose molecule that converts the COOH group into a COONa group to increase the ionic charges of the carboxylate groups and enhance agave CNF dispersion in water for the homogenization step. Figure created by Dr. Sunil Sharma through the use of ChemDraw software.

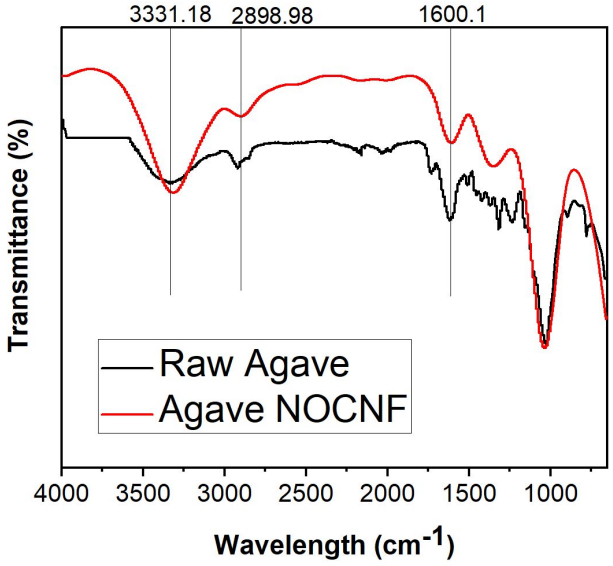

Figure 2. FTIR spectra of raw agave biomass (black) and agave CNF (red). The removal of impurities like lignin and hemicellulose was confirmed by the decrease or absence of peaks at 1600 cm^{-1}, 1730 cm^{-1}, 1490 cm^{-1}, 1290 $cm^{-1}$and 860 cm^{-1} in the spectrum for agave CNF. The OH stretching peak at 3331 cm^{-1} did not broaden in the agave CNF as compared to the corresponding peak for the raw agave biomass. This may be attributed to the absence of hydrogen bonding disturbance in the modification of C6 primary hydroxyl to carboxyl group in cellulose chains as described by Sharma et al., 2017. Figure created by competition entrant.

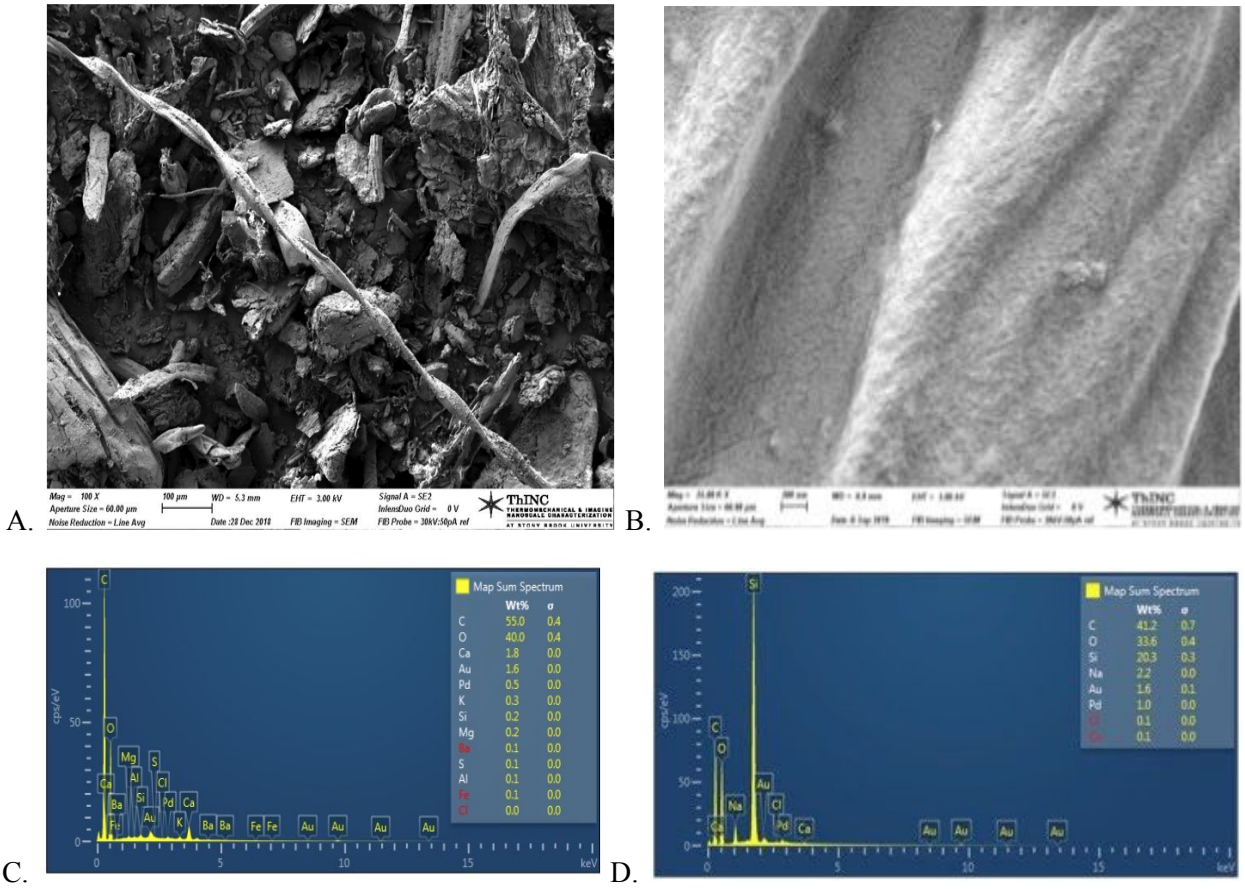

Figure 3. SEM and EDX images of raw agave biomass (A, C) and agave CNF (B, D). Raw agave biomass contains many impurities and crystalline structures visualised in the SEM image taken at a 200 nm scale. The impurities are not present in the SEM image taken at a 200 nm scale for agave CNF and are replaced by fibrous structures. This was supported by the EDX peaks for raw agave biomass and agave CNF. There are extracts of many elements from various impurities in the EDX diagram for raw agave biomass. The EDX diagram for agave CNF only has carbon and oxygen peaks from cellulose, sodium peak from conversion of COOH groups to COONa, and silicon peak from the silicon wafer used for imaging. Figure adapted by competition entrant from SEM and EDX machines in the Advanced Energy Research and Technology Center at Stony Brook University.

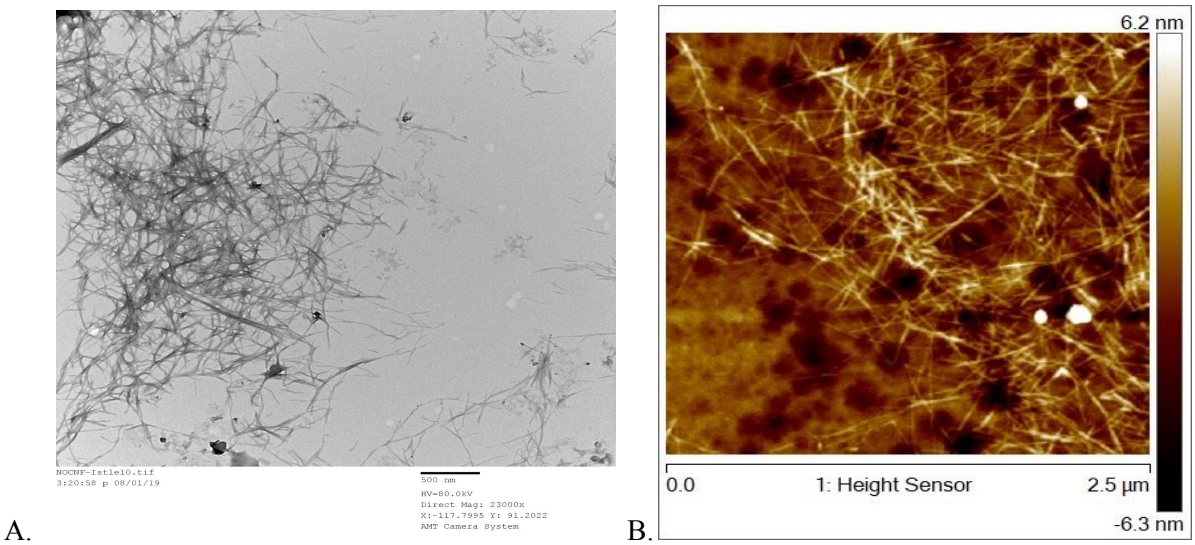

A. B.

Figure 4. TEM image of agave CNF (A) and AFM image of CNF (B). TEM images were obtained at magnification 395000X (A). ImageJ software was used to measure and average the length and width of 50 fibers. The average lengths of agave CNF within one standard deviation ranged from 122.28 to 359.758 nm and the average width of agave CNF was 5-6 nm. AFM was performed in non-contact mode on agave CNF to produce a corresponding 2D height image (B) and calculate the average thickness of agave CNF, which was 1.6 nm. The morphology measurements of average fiber length, width, and thickness for agave CNF were consistent with other forms of CNF. Figure adapted by competition entrant from TEM and AFM machines in the Advanced Energy Research and Technology Center at Stony Brook University.

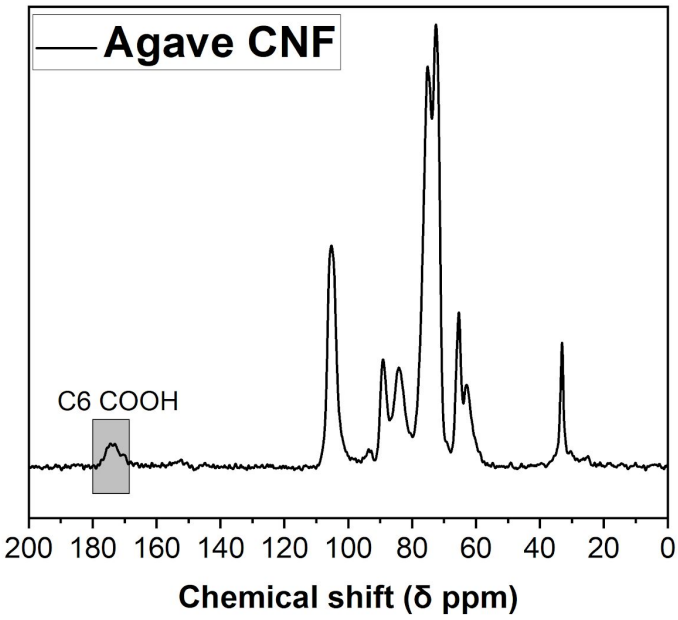

Figure 5. Solid state ^{13}C CPMAS NMR spectrum of agave CNF. The 6 main peaks on the spectrum represent the assembly of C1, C2, C3, C4, C5, and C6 carbons in the anhydroglucose units. The regional assignment of the C6 carbon confirmed the oxidation of the CH2OH functional group to the COOH functional group at the C6 position of the cellulose molecules in the raw agave biomass. The absence of peaks attributed to hemicellulose and lignin's guaiacyl and syringyl units further confirmed the removal of lignin and hemicellulose impurities in the raw agave biomass during the conversion to agave CNF. This also supports the role of nitric acid in removing impurities from the raw biomass during the nitro oxidation process. Figure adapted by competition entrant from ^{13}C CPMAS NMR machine in the Nuclear Magnetic Resonance Facility at Stony Brook University.

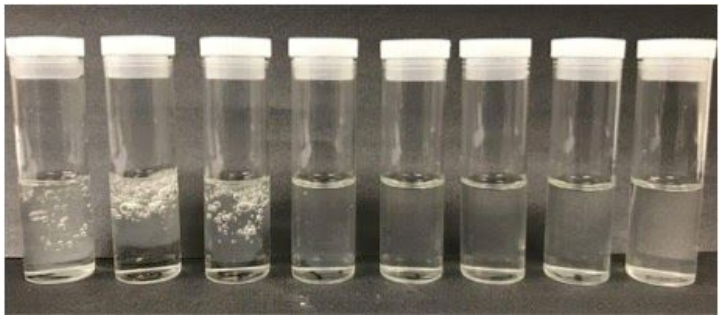

Figure 6. La^{3+} and agave CNF solutions. The concentrations of the La^{3+} ions from left to right are 500 ppm, 250 ppm, 100 ppm, 50 ppm, 25 ppm, 10 ppm, 5 ppm, and 2 ppm. The gelation effect is more visible in higher concentrations of La^{3+} ions. This supports the hypothesis there is cross-linking between the La^{3+} ions and agave CNF because higher concentrations of La^{3+} would have increased ions and therefore increased cross-linking. The observation of gelation prompted rheological analysis on the depicted solutions shown in Figure 11. Figure created by competition entrant.

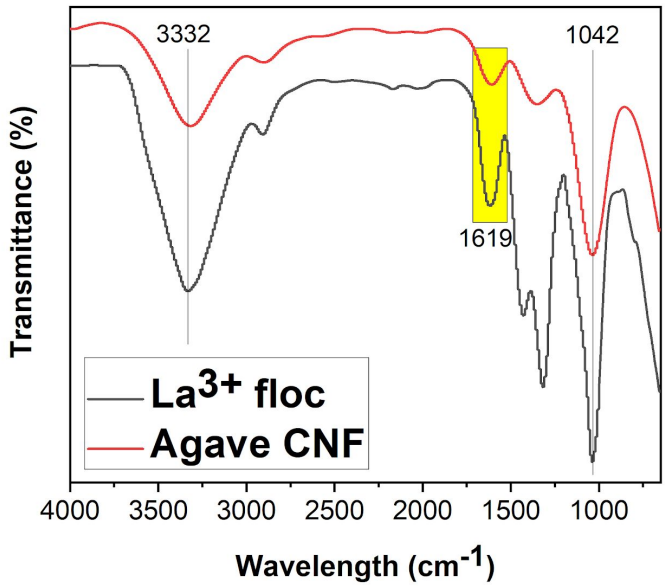

Figure 7. FTIR spectra of agave CNF and floc formed by agave CNF and La^{3+} ions. The broadening of the OH stretching peak at 3332 cm^{-1} on the floc spectrum as compared to the agave CNF spectrum indicates the formation of lanthanum hydroxide on the surface of agave CNF through cross-linking between the agave CNF and La^{3+} ions. This cross-linking effect is supported by the broadening of the COO^- peak at 1619 cm^{-1} on the floc spectrum as compared to the agave CNF spectrum. Figure created by competition entrant.

A. 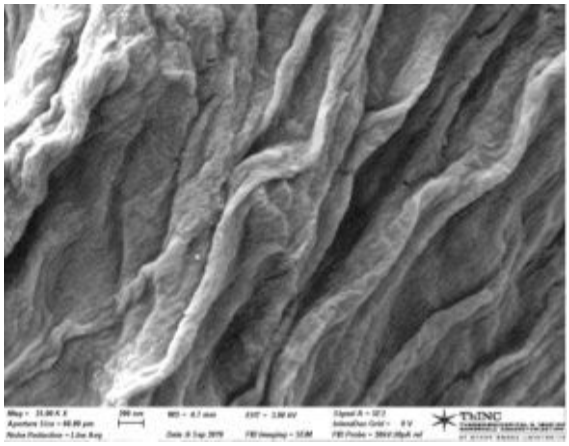 B. 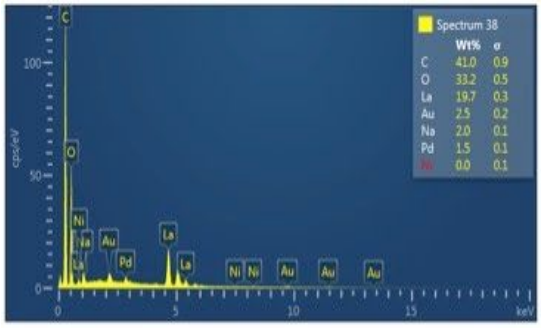

Figure 8. SEM image (A) and EDX diagram (B) of floc. The SEM/EDX performed on a floc formed by agave CNF and La^{3+} ions of concentration 500 ppm suggests further interaction between the La^{3+} ions and agave CNF surface functional groups. The SEM image of the floc (A) taken at a 200 nm scale has thick structures that can be associated with lanthanum oxide. This is supported by EDX diagram of the floc (B), where the lanthanum peaks can attributed to La^{3+} ions, the carbon, oxygen, and sodium peaks can be attributed to the agave CNF, and the gold peaks can be attributed to the gold sputter coating applied to the floc sample for imaging. Figure adapted by competition entrant from SEM and EDX machines in the Advanced Energy Research and Technology Center at Stony Brook University.

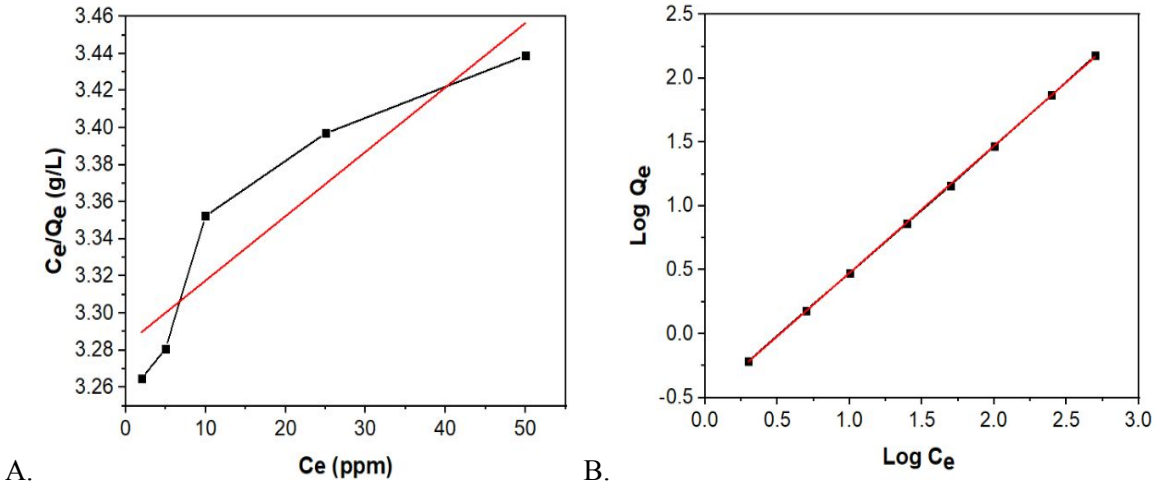

A. B.

Figure 9. Langmuir isotherm (A) and Freundlich isotherm (B) for La^{3+} ions by agave CNF. The red line represents the data points from ICP-MS studies and the black line represents the line of best fit calculated by the isotherm equations stated in Equation 1 and Equation 2 in section 3.3 of the Methodology. In the Langmuir isotherm model, $R^2 = 0.851916$, the slope of the line of best fit = 0.0035, and $Q_{max} = 285.714$. There is a moderate R^2 value for the Langmuir isotherm that represents a monolayer adsorption model. The Q_{max} value for agave CNF is compared to Q_{max} values for other lanthanide ion removal mechanisms in Table 1. In the Freundlich isotherm model, $R^2 = 0.99993$, the slope for the line of best fit = 0.9951, $K_f =$ 3.296856164, and n = 1.00492413. There is a very high R^2 value for the Freundlich isotherm that represents a multilayer adsorption model. The K_f and n values for agave CNF are compared to K_f and n values for other lanthanide ion removal mechanisms in Table 2. The high R^2 value for the Freundlich isotherm model may be explained by cross-linking between the La^{3+} ions and agave CNF which is explored with rheological analysis in Figure 11. Figures created by competition entrant.

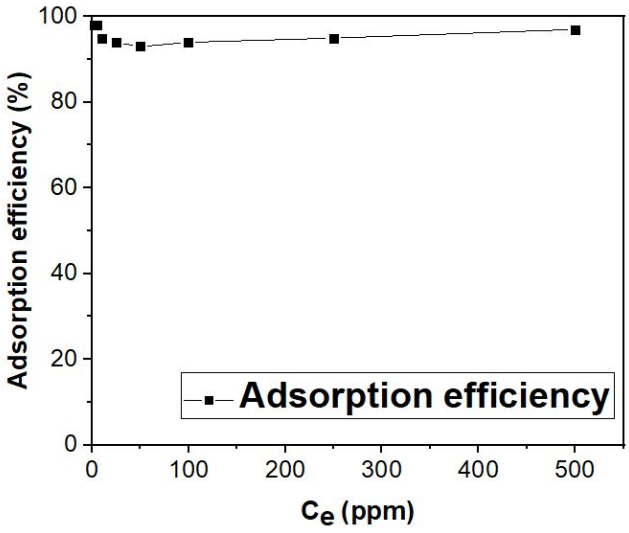

Figure 10. Adsorption efficiency of agave CNF for La^{3+} ions. The adsorption efficiency was calculated from the ICP-MS studies for each concentration of La^{3+} ions tested. The difference between the maximum La^{3+} ions contained in the solution for the concentration being tested and the La^{3+} detected in the decanted solution through ICP-MS was divided by the

maximum La^{3+} ions contained in the solution for the concentration being tested and then converted to a percentage. The percentage of adsorption efficiency is graphed against the concentration of the La^{3+} solution tested. There was over a 90% efficiency for all concentrations tested and listed in Figure 6. There is no trend in the adsorption efficiency as the concentration of the La^{3+} solution increase. Figure created by competition entrant.

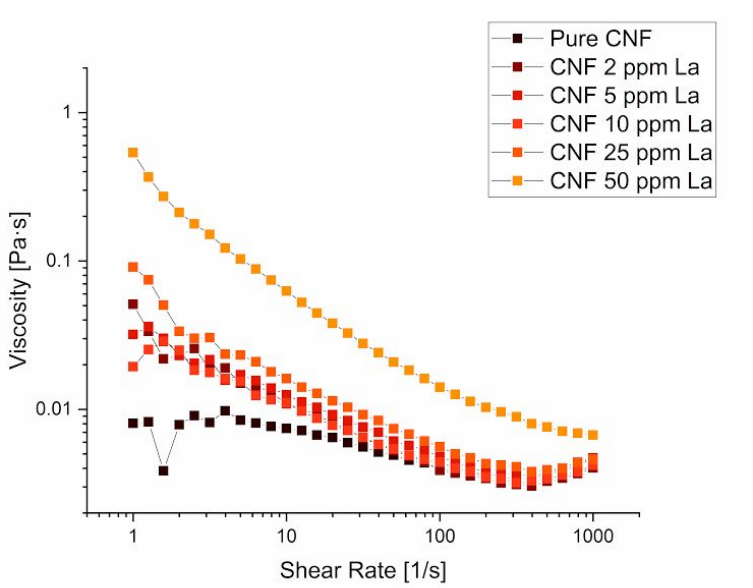

Figure 11. Rheological Analysis for agave CNF and La^{3+} ion solutions. The shear rate of the agave CNF and La^{3+} ions solutions was compared to their viscosity for solutions with the following La^{3+} ion concentrations: 0 ppm, 2 ppm, 5 ppm, 10 ppm, 25 ppm, and 50 ppm. There is a linearly negative relationship between the shear rate and viscosity of the solution for the lower concentration La^{3+} solutions, followed by an exponentially negative relationship between the shear rate and viscosity for the higher concentration La^{3+} solutions. This suggests a relationship between the La^{3+} ion solution's concentration and its viscosity that is similar to the relationship for CNF as demonstrated by Zhan et al., 2019. This relationship supports cross-linking between La^{3+} ions and agave CNF because the La^{3+} ions may also have a relationship with their overlap concentration. Specifically, La^{3+} ions may be screening the agave CNF surface with their positive charge, which attracts multiple COO^- groups and initiates cross-linking. Both agave CNF and La^{3+} display shear thinning behavior. Figure created by competition entrant.

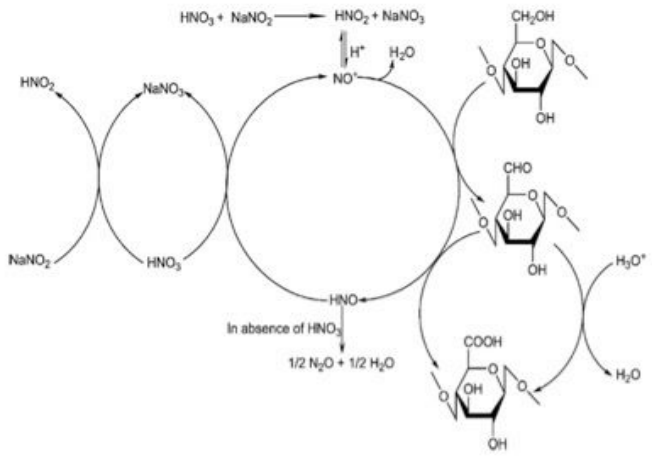

Figure 12. Proposed mechanism of the nitro oxidation process. The one-step nitro oxidation process utilizes nitric acid and sodium nitrite to both remove impurities in raw biomass like lignin and hemicellulose and oxidize the C6 position on the remaining cellulose molecules. Nitric acid is the primary agent in removing impurities in the biomass and also serves as a fibrillating agent to convert cellulose into nano-scale fibers. The addition of sodium nitrite forms HNO_2 ions that release NO^+ ions to oxidize cellulose at the C6 position and HNO to oxidize back into HNO_2 in acidic conditions and continue the oxidation cycle. Figure adapted from Sharma et al., 2017.

Table 1.

Q_{max} values for La^{3+} ion adsorption from Langmuir isotherm model.

Adsorbent Material	Q_{max} value (mg/g)	References
Platanus orientalis leaf powder	28.65	(Sert et al., 2008)
Mesoporous silica supports	35.5	(Yantasee, 2009)
Acid treated cellulose nanofibrils	47.8	(Oyewo, 2017)
Stichcoccus bacillaris	51.02	(Birungi, 2015)
Chlorella vulgaris	74.60	(Birungi, 2015)
Sargassum species	91.68	(Oliveira and Garcia, 2009)
Magnetic alginate chitosan gel beads	97.1	(Wu, 2010)
Desmodesmus multivariabilis	100	(Birungi, 2015)
Scenedesmus acuminutus	111.1	(Birungi, 2015)
Iron oxide loaded calcium alginate beads	123.5	(Wu, 2010)
Chloroidium saccharophilum	129.87	(Birungi, 2015)
Chlamydomonas reinhardtii	142.86	(Birungi, 2015)
Turbinaria conoides (brown algae)	154.7	(Vijayaraghavan, 2010)
Bamboo charcoal	214	(Chen, 2010)
Agave CNF	285.7	

Note. Adsorption capacities (mg/g) were represented as Q_{max} values calculated from Langmuir isotherm models. The Q_{max} values of La^{3+} ion adsorbent materials derived from biomass sources in previous literature were compared to the Q_{max} value calculated in this study. Agave CNF had a higher Q_{max} value and adsorption capacity than previously tested adsorbents for La^{3+} ion adsorption.

Table 2.

K_f and n values for La^{3+} ion adsorption from Freundlich isotherm model.

Adsorbent Material	K_f	n	References
Platanus orientalis leaf powder	6.33	3.14	(Sert et al., 2008)
Acid treated cellulose nanofibrils	23.3	7.14	(Oyewo, 2017)
Stichcoccus bacillaris	4.51	9.04	(Birungi, 2015)
Chlorella vulgaris	3.66	3.41	(Birungi, 2015)
Sargassum species	0.82	5.24	(Oliveira and Garcia, 2009)
Desmodesmus multivariabilis	4.93	4.17	(Birungi, 2015)
Scenedesmus acuminutus	4.259	3.50	(Birungi, 2015)
Bamboo charcoal	8.7	1.82	(Chen, 2010)
Chloroidium saccharophilum	4.81	4.06	(Birungi, 2015)
Chlamydomonas reinhardtii	4.721	3.35	(Birungi, 2015)
Turbinaria conoides (brown algae)	42.8	4.96	(Vijayaraghavan, 2010)
Agave CNF	3.297	1.004	

Note. Adsorption capacity was qualitatively represented as K_f and n value calculated from Freundlich isotherm models. The K_f and n values of La^{3+} ion adsorbent materials derived from biomass sources in previous literature were compared to the K_f and n values calculated in this study. Agave CNF had lower K_f and n values than previously tested adsorbents for La^{3+} ion adsorption.

7. References

1. Bernardinelli, O. D., Lima, M. A., Rezende, C. A., Polikarpov, I., & Deazevedo, E. R. (2015). Quantitative 13C MultiCP solid-state NMR as a tool for evaluation of cellulose crystallinity index measured directly inside sugarcane biomass. *Biotechnology for Biofuels*, *8*(1). doi: 10.1186/s13068-015-0292-1
2. Birungi, Z. S. (2015). Retrieved from https://pdfs.semanticscholar.org/5e51/8a02e1343e626bb7dfdf2057763348f9cd81.pdf
3. Chen, J., Li, C., Ristovski, Z., Milic, A., Gu, Y., Islam, M. S., … Dumka, U. C. (2017). A review of biomass burning: Emissions and impacts on air quality, health and climate in China. *Science of the Total Environment*, *579*, 1000–1034. doi: 10.1016/j.scitotenv.2016.11.025
4. Chen, Q. (2010). Study on the adsorption of lanthanum(III) from aqueous solution by bamboo charcoal. *Journal of Rare Earths*, *28*, 125–131. doi: 10.1016/s1002-0721(10)60272-4
5. Corbin, K. R., Byrt, C. S., Bauer, S., Debolt, S., Chambers, D., Holtum, J. A. M., … Burton, R. A. (2015). Prospecting for Energy-Rich Renewable Raw Materials: Agave Leaf Case Study. *Plos One*, *10*(8). doi: 10.1371/journal.pone.0135382
6. Drinking Water. (2019, June 14). Retrieved from https://www.who.int/news-room/fact-sheets/detail/drinking-water.
7. Habibi, Y. (2014). Key advances in the chemical modification of nanocelluloses. *Chem. Soc. Rev.*, *43*(5), 1519–1542. doi: 10.1039/c3cs60204d
8. Haque, N., Hughes, A., Lim, S., & Vernon, C. (2014). Rare Earth Elements: Overview of Mining, Mineralogy, Uses, Sustainability and Environmental Impact. *Resources*, *3*(4), 614–635. doi: 10.3390/resources3040614
9. Hidalgo-Reyes, M., Caballero-Caballero, M., Hernández-Gómez, L. H., & Urriolagoitia-Calderón, G. (2015). Chemical and morphological characterization of *Agave angustifolia*bagasse fibers. *Botanical Sciences*, *93*(4), 807. doi: 10.17129/botsci.250
10. Humphries, Marc. (2013). *Rare Earth Elements: The Global Supply Chain* (CRS Report No. 41347). Retrieved from Congressional Research Service website: https://fas.org/sgp/crs/natsec/R41347.pdf
11. Isogai, A. (2018). Development of completely dispersed cellulose nanofibers. *Proceedings of the Japan Academy, Series B*, *94*(4), 161–179. doi: 10.2183/pjab.94.012
12. Isogai, A., Saito, T., & Fukuzumi, H. (2011). TEMPO-oxidized cellulose nanofibers. *Nanoscale, 3(1), 71–85.* doi:10.1039/c0nr00583e
13. King, H. M. (n.d.). REE - Rare Earth Elements and their Uses. *Geology.com*.
14. Klemm, D., Kramer, F., Moritz, S., Lindström, T., Ankerfors, M., Gray, D., & Dorris, A. (2011).

Nanocelluloses: A New Family of Nature-Based Materials. *Angewandte Chemie International Edition*, *50*(24), 5438–5466. doi: 10.1002/anie.201001273

15. Krauklis, A. E. (2018). Use of Synthetic and Natural Zeolites Tailored for As(V) Sorption. *Zeolites and Their Applications*. doi: 10.5772/intechopen.72614
16. Li, K., Liang, T., Wang, L., & Tian, S. (2018). Inhalation exposure and potential health risk estimation of lanthanides elements in PM2.5 associated with rare earth mining areas: a case of Baotou city, northern China. *Environmental Geochemistry and Health*, *40*(6), 2795–2805. doi: 10.1007/s10653-018-0146-4
17. Liu, J., Plog, A., Groszewicz, P., Zhao, L., Xu, Y., Breitzke, H., … Buntkowsky, G. (2015). Design of a Heterogeneous Catalyst Based on Cellulose Nanocrystals for Cyclopropanation: Synthesis and Solid-State NMR Characterization. *Chemistry - A European Journal*, *21*(35), 12414–12420. doi: 10.1002/chem.201501151
18. Mahitha, U., Devi, G. D., Sabeena, M. A., Shankar, C., & Kirubakaran, V. (2016). Fast Biodegradation of Waste Cotton Fibres from Yarn Industry using Microbes. *Procedia Environmental Sciences*, *35*, 925–929. doi: 10.1016/j.proenv.2016.07.070
19. Mielenz, J. R., Rodriguez, M., Thompson, O. A., Yang, X., & Yin, H. (2015). Development of Agave as a dedicated biomass source: production of biofuels from whole plants. *Biotechnology for Biofuels*, *8*(1). doi: 10.1186/s13068-015-0261-8
20. National Academy Press. (1999). *Identifying future drinking water contaminants: based on the 1998 Workshop on Emerging Drinking Water Contaminants*. Washington, D.C.
21. Negrea, A., Gabor, A., Davidescu, C. M., Ciopec, M., Negrea, P., Duteanu, N., & Barbulescu, A. (2018). Rare Earth Elements Removal from Water Using Natural Polymers. *Scientific Reports,8*(1). doi:10.1038/s41598-017-18623-0
22. Oliveira, R., & Jr., O. G. (2009). Study of Biosorption of Rare Earth Metals (La, Nd, Eu, Gd) by *Sargassum* sp. Biomass in Batch Systems: Physicochemical Evaluation of Kinetics and Adsorption Models. *Advanced Materials Research*, *71-73*, 605–608. doi: 10.4028/www.scientific.net/amr.71-73.605
23. Oyewo, O. A. (2017). Retrieved from http://tutvital.tut.ac.za:8080/vital/access/manager/Repository/tut:4240
24. Pandey, B. D. (2012). *State-of-the-art Report On Technology For Producing Rare Metals in India* (Tech.).
25. Pereao, O., Bode-Aluko, C., Fatoba, O., Laatikaine, K., & Petrik, L. (2018). Rare earth elements removal techniques from water/wastewater: a review. *Desalination And Water Treatment*, *130*,

71–86. doi: 10.5004/dwt.2018.22844

26. Piotrwoski, S., & Carus, M. (2011). Multi-criteria evaluation of ligno- cellulosic niche crops for use in biorefinery processes. *Biocore*.
27. Proctor, A., & Toro-Vazquez, J. F. (1996). The Freundlich isotherm in studying adsorption in oil processing. *Journal of the American Oil Chemists' Society*, *73*(12), 1627–1633. doi: 10.1007/bf02517963
28. Rim, K. T., Koo, K. H., & Park, J. S. (2013). Toxicological Evaluations of Rare Earths and Their Health Impacts to Workers: A Literature Review. *Safety and Health at Work, 4*(1), 12-26. doi:10.5491/shaw.2013.4.1.12
29. Rosli, N. A., Ahmad, I., & Abdullah, I. (2013). Isolation and Characterization of Cellulose Nanocrystals from Agave angustifolia Fibre. *BioResources,8*(2).
30. Sert, S., Kütahlayi, C., Inan, S., Çetinkaya, B., & Eral, M. (2008). Biosorption of lanthanum and cerium from aqueous solutions by Platanus orientalis leaf powder. *Hydrometallurgy*, *90*(1), 13–18. doi: 10.1016/j.hydromet.2007.09.006
31. Sharma, P. R., Chattopadhyay, A., Sharma, S. K., Geng, L., Amiralian, N., Martin, D., & Hsiao, B. S. (2018). Nanocellulose from Spinifex as an Effective Adsorbent to Remove Cadmium(II) from Water. *ACS Sustainable Chemistry & Engineering*, *6*(3), 3279–3290. doi: 10.1021/acssuschemeng.7b03473
32. Sharma, P. R., Joshi, R., Sharma, S. K., & Hsiao, B. S. (2017). A Simple Approach to Prepare Carboxycellulose Nanofibers from Untreated Biomass. *Biomacromolecules,18*(8), 2333-2342. doi:10.1021/acs.biomac.7b00544
33. Vijayaraghavan, K., Sathishkumar, M., & Balasubramanian, R. (2010). Biosorption of Lanthanum, Cerium, Europium, and Ytterbium by a Brown Marine Alga,Turbinaria Conoides. *Industrial & Engineering Chemistry Research*, *49*(9), 4405–4411. doi: 10.1021/ie1000373
34. Wang, D. (2018). A critical review of cellulose-based nanomaterials for water purification in industrial processes. *Cellulose,26*(2), 687-701. doi:10.1007/s10570-018-2143-2
35. Wu, D., Zhao, J., Zhang, L., Wu, Q., & Yang, Y. (2010). Lanthanum adsorption using iron oxide loaded calcium alginate beads. *Hydrometallurgy*, *101*(1-2), 76–83. doi: 10.1016/j.hydromet.2009.12.002
36. Yantasee, W., Fryxell, G. E., Addleman, R. S., Wiacek, R. J., Koonsiripaiboon, V., Pattamakomsan, K., … Raymond, K. N. (2009). Selective removal of lanthanides from natural waters, acidic streams and dialysate. *Journal of Hazardous Materials*, *168*(2-3), 1233–1238. doi: 10.1016/j.jhazmat.2009.03.004

37. Zhan, C., Sharma, P. R., Geng, L., Sharma, S. K., Wang, R., Joshi, R., & Hsiao, B. S. (2019). Structural characterization of carboxyl cellulose nanofibers extracted from underutilized sources. *Science China Technological Sciences*, *62*(6), 971–981. doi: 10.1007/s11431-018-9441-1